PHOTONICS Research

Facile active control of a pulsed erbium-doped fiber laser using modulation depth tunable carbon nanotubes

Xintong Xu,[1,2] Shuangchen Ruan,[1,*] Jianpang Zhai,[1] Ling Li,[1] Jihong Pei,[2] and Zikang Tang[3]

[1]Shenzhen Key Laboratory of Laser Engineering, Guangdong Provincial Key Laboratory of Micro/Nano Optomechatronics Engineering, Shenzhen University, Shenzhen 518060, China
[2]College of Information Engineering, ATR National Defence S&T Key Laboratory, Shenzhen University, Shenzhen 518060, China
[3]Institute of Applied Physics & Materials Engineering, Faculty of Science and Technology, University of Macau, Macau, China
*Corresponding author: scruan@szu.edu.cn

Received 12 June 2018; revised 31 August 2018; accepted 31 August 2018; posted 5 September 2018 (Doc. ID 335051); published 12 October 2018

Short pulsed fiber lasers have been widely made using single-walled carbon nanotubes as a saturable absorber (SA). However, most of the currently used devices can only operate in one determined operation state with an unchangeable modulation SA depth in the cavity, which significantly limits their application in photonic devices. In this paper, well-aligned carbon nanotube arrays are synthesized using zeolite $AlPO_4$-5 as a template, which features anisotropic optical absorption. The linear optical absorption of the as-synthesized carbon nanotube arrays can easily be tuned by adjusting a polarization controller, thus providing a tunable modulation depth for the carbon nanotube SA. By exploiting this SA in an erbium-doped fiber laser cavity, both *Q*-switched and mode-locked pulsed lasers are achieved by simply adjusting a polarization controller under a fixed pump power of 330 mW. In addition, the repetition rate of the *Q*-switching and pulse duration of the mode-locking can be tuned according to the variation of modulation depth. Moreover, soliton molecules can be obtained when the modulation depth of the SA is 4.5%. © 2018 Chinese Laser Press

https://doi.org/10.1364/PRJ.6.000996

1. INTRODUCTION

Single-walled carbon nanotubes (SWCNTs) have extraordinary optical and electronic properties that make them attractive for numerous applications [1–4]. Recently, carbon nanotubes have been widely used as saturable absorbers (SAs) in pulsed fiber lasers owing to their large saturable absorption, ultrafast recovery time, and broadband operation [5–10]. To date, SWCNT-based SAs have been successfully used for mode-locking and *Q*-switching in fiber lasers, in which the operating wavelength ranges from 1.0 to 2.0 μm. Normally, mode-locked fiber lasers can generate pulses with ultra-short duration, while *Q*-switched fiber lasers can generate pulses with high energy. Therefore, fiber lasers with different laser operation states in a fixed laser cavity are urgently needed. Generally, carbon nanotubes are embedded in polymer matrices to form SWCNT-polymer SAs, leading to the random orientation of the carbon nanotubes [11–14]. In this condition, the absorption of the carbon nanotubes is fixed when they are inserted into a laser cavity, leading to a fixed modulation depth of the SA. Thus, the fiber laser is limited to a single laser-operation state, mode-locking or *Q*-switching, which significantly restricts its application. To promote the application of carbon nanotube SAs, it is important to develop a facile method to control the modulation depth, which is the key parameter for the realization of fiber lasers with several different laser operations [15–17].

The results of previous works have demonstrated that the modulation depth can be changed by adjusting SA absorption [15,18,19]. Well-aligned carbon nanotube arrays have an excellent anisotropic response to optical radiation due to their constrained electron motion and electron–phonon coupling. On this basis, polarization-sensitive optical devices based on well-aligned carbon nanotube arrays have been developed [20–22]. Thus, well-aligned carbon nanotube array SAs may provide a method to control the operation state of pulsed lasers by adjusting the polarization state in the laser cavity based on their polarized absorption property.

In our previous work, well-aligned carbon nanotube arrays were fabricated inside the channels of zeolite $AlPO_4$-5 (AFI) single crystals, which exhibited very specific properties such as one-dimensional superconductivity and anisotropic optical absorption [23–25]. In this paper, well-aligned carbon nanotube arrays fabricated in AFI channels are used as polarization-sensitive SAs for the manipulation of the operation state of pulsed lasers. The as-synthesized well-aligned carbon nanotube

arrays have polarized optical absorption, which makes them highly suitable as a polarization-sensitive SA. *Q*-switching with different repetition rates, mode-locking with different pulse durations, and soliton molecules can be easily achieved by controlling modulation depth of the carbon nanotube SAs through adjustment of a polarization controller under a fixed pump power of 330 mW.

2. EXPERIMENTAL SECTION

A. Synthesis of AFI Single Crystals and Well-Aligned Carbon Nanotube Arrays

AFI crystals were used as the template to synthesize well-aligned carbon nanotube arrays by pyrolyzing tripropylamine (TPA) precursor in its one-dimensional channels. AFI is a well-known porous material which has a hexagonal structure with the space group of *P6cc*. Its framework consists of one-dimensional 12-ring channels that are packed parallel to the *c* axis. The AFI crystals were hydrothermally synthesized using a composite starting gel: $1.0Al_2O_3$:$1.0P_2O_5$:1.2TPA:$800H_2O$:0.8HF. During fabrication, aluminum tri-isopropoxide, which was used as a source of aluminum, was dissolved in water and stirred for 12 h. Then, orthophosphoric acid, which was used as a source of phosphorus, was added to the solution and stirred for 3 h. Similarly, the TPA that was used as an organic template was also added to the solution and stirred for 3 h. Subsequently, a diluted HF was added to the solution and stirred for 3 h. Finally, the solution was sealed in a Teflon-lined stainless-steel autoclave and heated to 175°C for 24 h. The AFI crystals were obtained after crystallization. The TPA containing the AFI single crystals was dehydrated at 873 K in a vacuum of 10^{-3} mbar for 4 h to form well-aligned carbon nanotube arrays. The Raman spectrum of SWCNTs@AFI was obtained using a Horiba Jobin-Yvon LabRan HR800 with a 514.5 nm laser excitation source.

B. Experimental Setup of the Erbium-Doped Fiber Laser

The laser setup of the erbium-doped fiber laser (EDFL) is shown in Fig. 1. A 1.0 m heavily erbium-doped fiber was used as the gain medium and pumped using a 980 nm diode through a fused wavelength division multiplexer. An optical isolator was used to ensure unidirectional operation. A polarization controller composed of a half-wave plate and two quarter-wave plates was used to tune the polarization state in the laser cavity. The total cavity length is about 8.6 m, and a 10% port extracted the pulses from the cavity. An optical spectrum analyzer (OSA) with a resolution of 0.05 nm, a 1 GHz high-speed oscilloscope, and an autocorrelator (Pulsecheck SM1200) were used to measure the optical pulse.

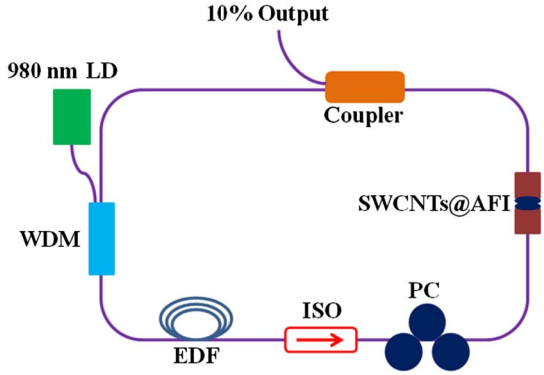

Fig. 1. Schematic diagram of the erbium-doped fiber laser.

3. EXPERIMENTAL RESULTS

First, AFI crystals were synthesized using a hydrothermal method. Then, the SWCNTs were obtained by pyrolyzing the TPA precursor. Figure 2(a) shows a scanning electron microscope image of the AFI single crystals. AFI is a type of porous material which contains one-dimensional channels packed in a hexagonal array, with an inner diameter of 0.73 nm [25], as seen in Fig. 2(b). The well-aligned SWCNTs are sketched inside of the AFI nanochannels, as shown in Fig. 2(c). Figure 2(d) shows the Raman spectrum of the SWCNTs fabricated in the channels of the AFI single crystal. In the low-frequency region (400–600 cm^{-1}), the Raman lines at 510 and 542 cm^{-1} are attributed to the A_{1g} radial breaking mode of the chiral (4,2) nanotube and the zigzag (5,0) nanotube, respectively [26–28]. The D bands in the central region (1000–1500 cm^{-1}) are characteristic of the disorder. The tangential G bands in the high-frequency region (1500–1620 cm^{-1}) are characteristic of carbon bond vibrations.

Based on the polarized optical absorption of well-aligned SWCNTs that were fabricated in the nanochannels of the AFI [27], the polarization-dependent saturable absorption of SWCNTs@AFI was measured using a homemade fs mode-locked EDFL (center wavelength of 1563 nm, pulse duration of 260 fs, repetition rate of 25 MHz). Figure 3(a) shows the schematic setup used for the measurement. The polarization controller (PC) was used to adjust the polarization state of the pulsed laser. For a fixed optical pump power, the PC was adjusted to change the values between power meters A and B. The maximum difference value between power meters A and B indicates the orthogonality between the laser polarization

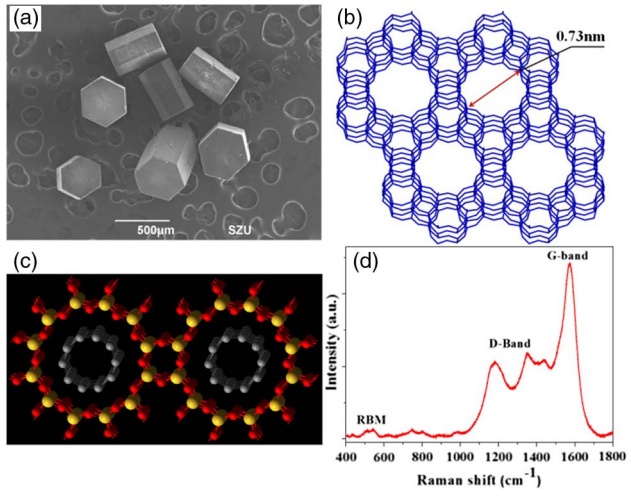

Fig. 2. (a) Scanning electron microscopy image of pristine AFI single crystals. (b) Framework structure of an AFI single crystal viewed along the [001] direction. (c) SWCNTs are sketched inside the channels of AFI. (d) Raman spectrum of the SWCNTs@AFI single crystal.

direction and the carbon nanotube axis ($E\|C$), while the minimum difference value indicates the parallel relationship between the laser polarization direction and the carbon nanotube axis ($E\perp C$) for polarized optical absorption of well-aligned SWCNTs. Thus, the modulation depth of the SWCNTs@AFI can be obtained in the cases of $E\|C$ and $E\perp C$. The nonlinear fitting of the experimental results shows that the modulation depth is 14% for $E\|C$ and 4.5% for $E\perp C$, as shown in Figs. 3(b) and 3(c), respectively. This finding clearly illustrates that these well-aligned carbon nanotubes are SAs with a tunable modulation depth, which is an ideal SA for a switchable pulsed laser. Moreover, the polarized absorption of well-aligned carbon nanotube arrays is shown in Fig. 3(d) using a polarized optical source. It is observed that the intensity of the optical absorption gradually increases with decreasing polarization angle θ from 90° to 0° (where θ is the polarization angle from the light polarized axis to the tube axis). The polarization-dependent absorption property of the carbon nanotube SAs is attributed to their constrained electron motion and electron–phonon coupling. Since the carbon nanotubes are well-aligned and well-separated from each other, only the electric field perpendicular to the nanotube axis is perfectly screened, and thus any light component polarized along the tube axis will experience the largest absorption.

Finally, an AFI single crystal that hosted the SWCNTs was used as the SA, which was placed between two fiber connectors and then integrated into the EDFL cavity. Figure 1 shows a schematic diagram of the erbium-doped ring-cavity fiber laser.

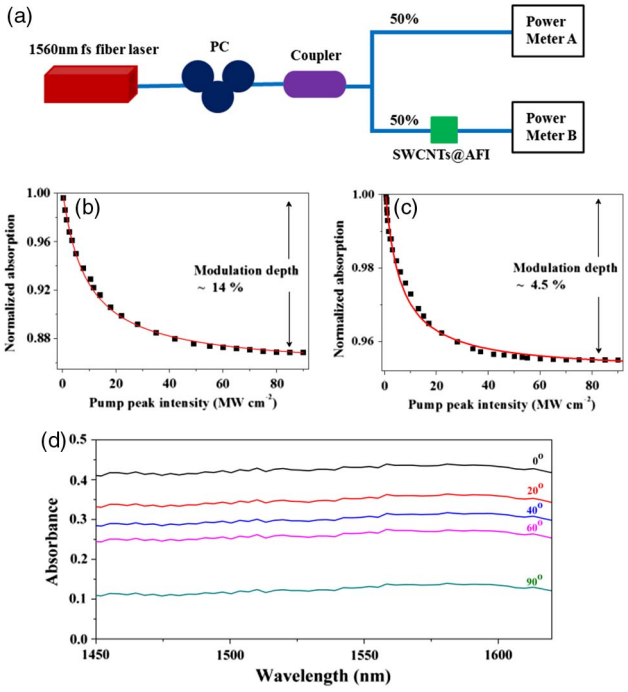

Fig. 3. (a) Experimental setup for the measurement of saturable absorption of SWCNTs@AFI. Dots are the measured data and the red line is the data fitting. Pulse excitation wavelength at 1.5 μm with different polarization directions (b) $E\|C$ and (c) $E\perp C$. (d) Polarized absorption spectra of the well-aligned carbon nanotube arrays under different polarization angles.

The insertion loss and polarization-dependent loss of the well-aligned carbon nanotube array SA were measured to be ~3 and ~21 dB, respectively. Such a high polarization-dependent loss further illustrates that the well-aligned carbon nanotube arrays can be used as polarization-sensitive SAs for the manipulation of the operation state of pulsed lasers. First, a continuous-wave laser was obtained using a pump power of 310 mW. Then, the PC was adjusted to maintain a minimum output power. Under this condition, the light with linear polarization parallel to the axis of the carbon nanotubes can be confirmed for the maximum optical absorption of the carbon nanotubes. Thereafter, only the half-wave plate was adjusted in the following experiment to ensure the light that passed through the carbon nanotubes is linearly polarized, which can be clearly verified by the following phenomenon. The output power reaches a maximum value after rotation of the half-wave plate by 45°, which indicates orthogonality between the optical polarization direction and the axis of the carbon nanotubes. Thus, it is possible to control the polarization angle θ (θ is the polarization angle measured from the light-polarized axis to the tube axis) by rotating the half-wave plate. Initially, the PC was adjusted to ensure that $E\|C$ was achieved. A Q-switched pulsed laser was thus obtained at the pump power of 330 mW. Figure 4(a) shows the Q-switched pulse train where the repetition rate is 23.0 kHz. At a fixed pump power of 330 mW, through gradual adjustment of the PC, the repetition rate can be changed from 23 to 39.7 kHz, as shown in Fig. 4. It is observed that during this evolution process, the Q-switching operation remains highly stable at its uniform pulse peak intensity.

Figure 5 shows the pulse duration and average output power as functions of the polarization angle. By increasing this angle, the pulse duration becomes progressively shorter and the average output power increases. Figure 6(a) shows the internal fine structure of the optical pulse with more sampling points when the repetition rate of the Q-switching is 39.7 kHz. In this case, the pulse duration is about 4.2 μs. Figure 6(b) represents the

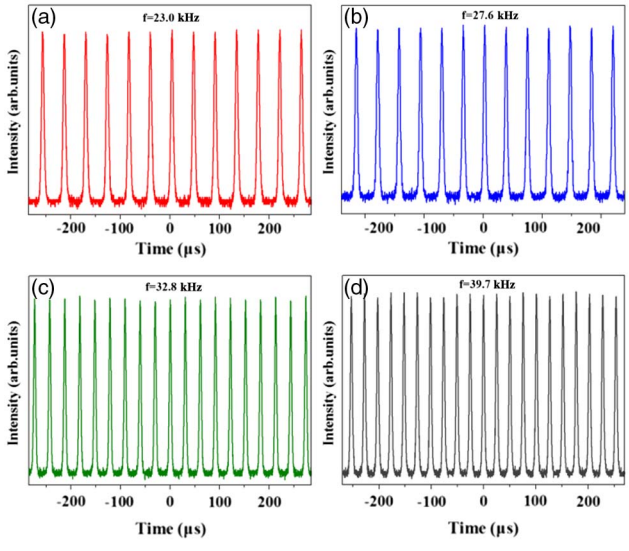

Fig. 4. Typical oscilloscope traces of the Q-switching pulse trains under different polarization angles of (a) 0°, (b) 8°, (c) 14°, and (d) 20°.

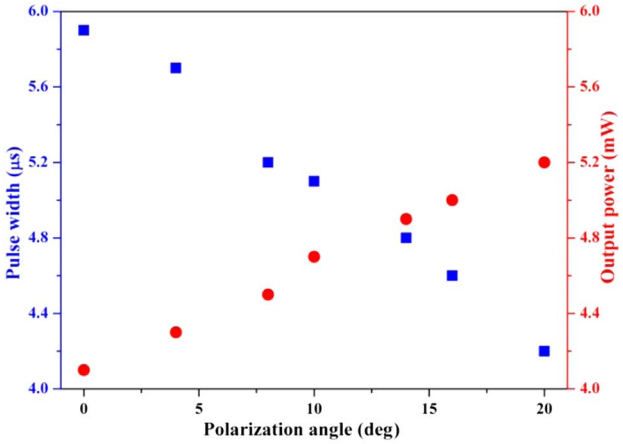

Fig. 5. Pulse duration and average output power as functions of polarization angle.

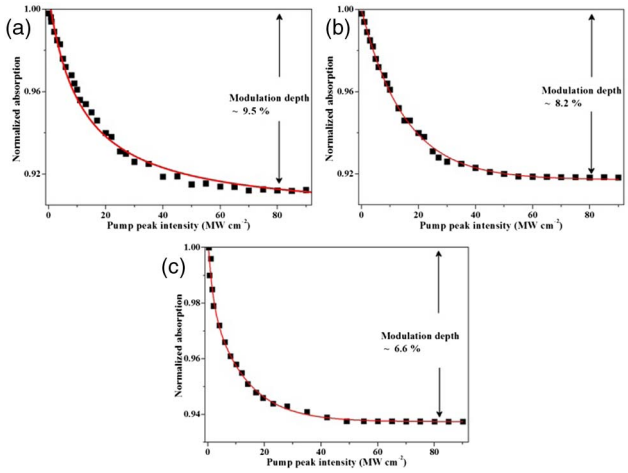

Fig. 7. Saturable absorption properties of the SWCNTs@AFI SA under different polarization angles of (a) 20°, (b) 40°, and (c) 70°.

corresponding spectrum measured by the OSA with a resolution of 0.02 nm. The central wavelength is about 1565.8 nm, and the 3 dB spectral width is about 0.67 nm.

The modulation depth of the SWCNTs changed from 14% to 9.5% after rotation of the half-wave plate by 10° [Figs. 3(b) and 7(a)]. Normally, a *Q*-switching laser has a tunable repetition that is dependent on the cavity gain and loss [17]. The relationship between the optical polarization direction and the axis of the carbon nanotubes is deviated from $E \| C$ by adjusting the PC. Thus, both the cavity loss and modulation depth of the SWCNTs decrease, leading to the increase of the repetition rate. With further adjustment of the PC after rotating the half-wave plate by 15°, the *Q*-switching state became unstable and eventually disappeared. Interestingly, stable mode-locked pulses were obtained by adjusting the PC via rotation of the half-wave plate by 20°. The corresponding polarization angle is 40°. The modulation depth of the SA was measured at about 8.2% under this condition [Fig. 7(b)].

Figure 8(a) shows the output pulse trains of the mode-locked EDFL. The repetition rate is 23.2 MHz (period $\tau = 43$ ns), as determined by the cavity length. Figure 8(b) shows the corresponding emission spectrum of the laser, which is soliton mode-locked for its Kell bands in the spectrum [29]. The operating central wavelength is about 1563.1 nm and the corresponding 3 dB spectral width is about 5.51 nm. The pulse width is about 386 fs, assuming a sech^2 pulse profile, as shown in Fig. 8(c). Figure 8(d) shows the radiofrequency (RF) spectrum of the laser output. The signal to noise ratio is about

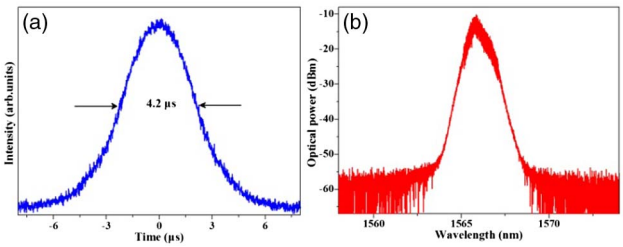

Fig. 6. Output characteristic of the EDFL operated in the *Q*-switching state. (a) Single pulse profile. (b) Emission spectrum.

67 dB at a resolution of 1 kHz, which indicates good stability of the mode-locked laser.

The 3 dB spectral width of the laser output is continuously tunable from 5.51 to 3.75 nm by further adjustment of the PC via rotation of the half-wave plate from 20° to 35° at the fixed pump power of 330 mW [Figs. 8(b) and 9], while the corresponding pulse duration varied from 386 to 863 fs [Figs. 8(c) and 9]. In addition, the modulation depth of the SWCNTs changed from 8.2% to 6.6% [Figs. 7(b) and 7(c)] during the pulse width expanding via rotation of the half-wave plate from 20° to 35°. A similar phenomenon has been reported in Ref. [18], which illustrates that the spectral bandwidth of the mode-locked pulse will be decreased by decreasing the modulation depth. Interestingly, a soliton molecular pair could be obtained after rotating the half-wave plate by 45°. In this case, the modulation depth was measured at about 4.5% [Fig. 2(c)], indicating the $E \perp C$ condition. The optical spectrum of Fig. 10(a) combined with the optical autocorrelation

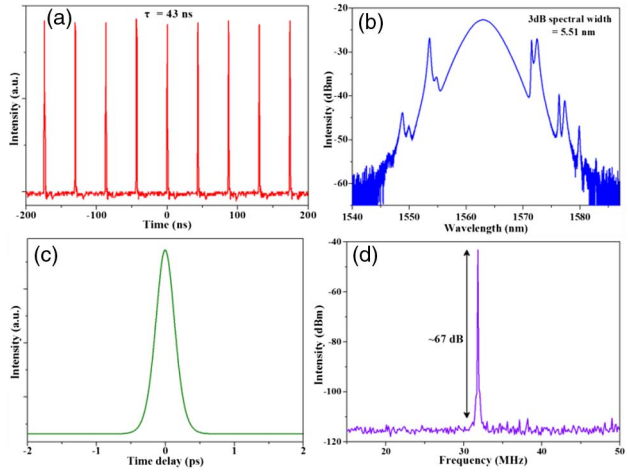

Fig. 8. Output characteristic of the EDFL operated in the mode-locking state. (a) Pulse train. (b) Emission spectrum. (c) Single pulse profile. (d) Radiofrequency spectrum.

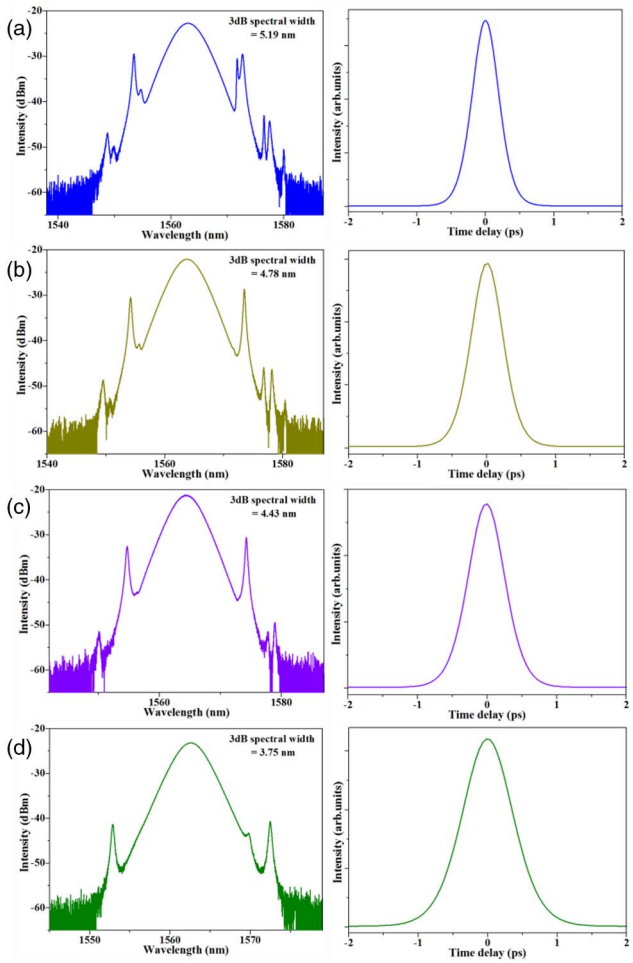

Fig. 9. Optical spectrum and corresponding single pulse profile of mode-locking under different polarization angles of (a) 46°, (b) 52°, (c) 60°, and (d) 70°.

trace of Fig. 10(b) demonstrates phase locking of the two bound solitons. The spectrum exhibits a central dip at the wavelength of 1562 nm, with a clear modulation period of 3 nm. The corresponding autocorrelation trace has the same width as the three peaks with an intensity ratio of 1:2:1, which indicates that the two bound solitons have the same intensity, pulse duration, and a constant separation. The single-pulse width is about 0.9 ps, fitted by the sech^2 profile. The pulse-to-pulse separation of the solitons is about 2.63 ps, which corresponds to the period of the spectral modulation. Figure 10(c) is the oscilloscope trace of the bound solitons. The interval between the two peaks is about 43 ns, which corresponds to a fundamental repetition rate of 23.2 MHz. Figure 10(d) shows the RF spectrum of the bound-state solitons. The signal-to-noise ratio is about 60 dB, which indicates the relatively high stability of the soliton molecule. The results of previous works have demonstrated that the traditional soliton can be switched to a bound soliton by simply increasing the pump power in the same fiber laser system [30–34]. In our laser system, the shift in the operation state from the traditional soliton to the bound soliton could be due to the decrease of loss. The bound-soliton operation can be obtained when the polarization of light is

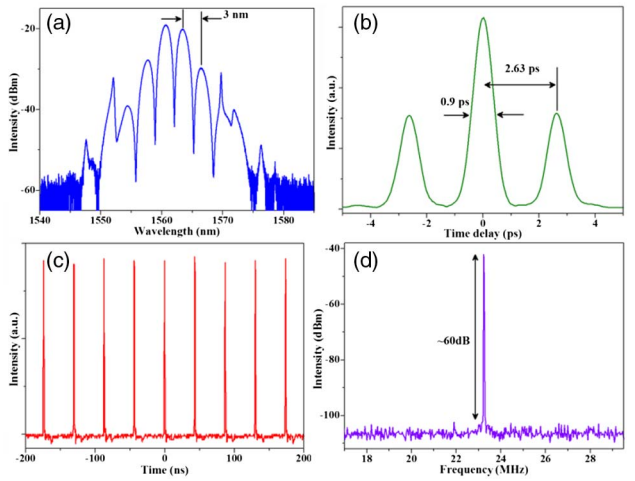

Fig. 10. (a) Emission spectrum, (b) autocorrelation trace, (c) pulse train, and (d) radiofrequency spectrum of two bound soliton EDFL.

perpendicular to the nanotube axis. Under this condition ($E \perp C$), the minimum optical absorption of the carbon nanotubes has the lowest loss in the cavity, while the pump power is kept unchanged. Thus, the mode-locked pulse laser would be over-driven by sudden decreases in the intra-cavity loss while maintaining the intra-cavity gain, leading to the switching of the laser operation state from traditional to bound soliton.

Nonlinear polarization evolution (NPE) is another technology that can be used to produce a mode-locked laser operation state, which normally requires two sets of polarization controllers or a polarization-dependent isolator in the fiber laser cavity [35–38]. Thus, the proposed setup with one PC and a polarization-independent isolator that was used in our fiber laser cavity may not be readily amenable to the mode-locked laser operation state based on an NPE mechanism. In addition, the NPE mode-locked fiber laser is sensitive to environmental perturbations and can be easily destroyed, whereas our mode-locked laser can maintain several days. Moreover, in order to completely exclude the effect of NPE that may contribute to the mode-locked laser operation in our fiber laser, the SA was purposely removed from the cavity to verify whether the pulsed operation was caused by the well-aligned carbon nanotube array SA. In this condition, only continuous-wave (CW) operation was obtained even if the pump power and the PC were changed over a large range (Fig. 11). Thus, based on our experimental results, the effect of NPE is negligible in comparison

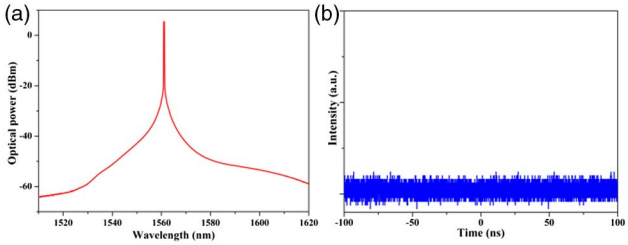

Fig. 11. (a) CW laser output spectrum of the EDFL without a carbon nanotube SA in the cavity. (b) Laser intensity as a function of time.

to the effect of the well-aligned carbon nanotube array SA in our fiber laser cavity.

4. CONCLUSION

Well-aligned single-walled carbon nanotube arrays were synthesized in the nanochannels of zeolite AFI, which can be used as a polarization-sensitive SA to manipulate a pulsed EDFL based on the polarized optical absorption property. The modulation depth of the SA can be changed from 14% to 4.5% by adjusting the polarization state from $E \| C$ to $E \perp C$. Using such a tunable modulation depth SA, both Q-switching and mode-locking optical pulses can be generated by simply adjusting the PC for a fixed 330 mW pump power. The repetition rate of the Q-switching and the pulse width of the mode-locking pulses can be manipulated by adjustment of the PC. Moreover, soliton molecules can also be observed under the same pump power of 330 mW. Our research demonstrates the efficacy of a modulation-depth tunable photonics material for manipulating pulsed laser operation.

Funding. National Key Research and Development Program of China (2016YFA0401100); National Natural Science Foundation of China (NSFC) (61575129, 61705134); Shenzhen Science and Technology Project (JCYJ20160328144942069); China Postdoctoral Science Foundation (2017M612723).

REFERENCES

1. S. Lijima and T. Ichihashi, "Single-shell carbon nanotubes of 1-nm diameter," Nature **364**, 737 (1993).
2. L. Wen, F. Li, and H. M. Cheng, "Carbon nanotubes and graphene for flexible electrochemical energy storage: from materials to devices," Adv. Mater. **28**, 4306–4337 (2016).
3. M. F. De Volder, S. H. Tawfick, R. H. Baughman, and A. J. Hart, "Carbon nanotubes: present and future commercial applications," Science **339**, 535–539 (2013).
4. P. Avouris, M. Freitag, and V. Perebeinos, "Carbon-nanotube photonics and optoelectronics," Nat. Photonics **2**, 341–350 (2008).
5. M. Chernysheva, A. Rozhin, Y. Fedotov, C. Mou, R. Arif, S. M. Kobtsev, E. M. Dianov, and S. K. Turitsyn, "Carbon nanotubes for ultrafast fibre lasers," Nanophotonics **6**, 1–30 (2017).
6. W. S. Kwon, H. Lee, J. H. Kim, J. Choi, K. S. Kim, and S. Kim, "Ultrashort stretched-pulse L-band laser using carbon-nanotube saturable absorber," Opt. Express **23**, 7779–7785 (2015).
7. J. Wang, Y. Yan, A. P. Zhang, B. Wu, Y. Shen, and H. Y. Tam, "Tunable scalar solitons from a polarization-maintaining mode-locked fiber laser using carbon nanotube and chirped fiber Bragg grating," Opt. Express **24**, 22387–22394 (2016).
8. Y. Wang, S. U. Alam, E. D. Obraztsova, A. S. Pozharov, S. Y. Set, and S. Yamashita, "Generation of stretched pulses and dissipative solitons at 2 μm from an all-fiber mode-locked laser using carbon nanotube saturable absorbers," Opt. Lett. **41**, 3864–3867 (2016).
9. M. Tsuzuki, L. Jin, M. Yamanaka, V. Sonnenchein, H. Tomita, A. Sato, T. Ohara, Y. Sakakibara, E. Omoda, H. Kataura, T. Iguchi, and N. Nishizawa, "Midinfrared optical frequency comb based on difference frequency generation using high repetition rate Er-doped fiber laser with single wall carbon nanotube film," Photon. Res. **4**, 313–317 (2016).
10. Y. Zhou, J. Lin, X. Zhang, L. Xu, C. Gu, B. Sun, A. Wang, and Q. Zhan, "Self-starting passively mode-locked all fiber laser based on carbon nanotubes with radially polarized emission," Photon. Res. **4**, 327–330 (2016).
11. S. Kobtsev, A. Ivanenko, Y. G. Gladush, B. Nyushkov, A. Kokhanovskiy, A. S. Anisimov, and A. G. Nasibulin, "Ultrafast all-fibre laser mode-locked by polymer-free carbon nanotube film," Opt. Express **24**, 28768–28773 (2016).
12. L. Hou, H. Guo, Y. Wang, J. Sun, Q. Lin, Y. Bai, and J. Bai, "Sub-200 femtosecond dispersion-managed soliton ytterbium-doped fiber laser based on carbon nanotubes saturable absorber," Opt. Express **26**, 9063–9070 (2018).
13. J. Koo, Y. W. Song, and J. H. Lee, "A carbon nanotube-embedded fiber-optic tunable coupler for flexible repetition rate control of a passively Q-switched fiber laser," Laser Phys. **24**, 045105 (2014).
14. H. H. Liu, K. K. Chow, S. Yamashita, and S. Y. Set, "Carbon-nanotube-based passively Q-switched fiber laser for high energy pulse generation," Opt. Laser Technol. **45**, 713–716 (2013).
15. E. J. Lee, S. Y. Choi, H. Jeong, N. H. Park, W. Yim, M. H. Kim, J. K. Park, S. Son, S. Bae, S. J. Kim, K. Lee, Y. H. Ahn, K. J. Ahn, B. H. Hong, J. Y. Park, F. Rotermund, and D. I. Yeom, "Active control of all-fibre graphene devices with electrical gating," Nat. Commun. **6**, 6851 (2015).
16. Q. Sheng, M. Feng, W. Xin, T. Han, Y. Liu, Z. Liu, and J. Tian, "Actively manipulation of operation states in passively pulsed fiber lasers by using graphene saturable absorber on microfiber," Opt. Express **21**, 14859–14866 (2013).
17. Y. Chen, G. Jiang, S. Chen, Z. Guo, X. Yu, C. Zhao, H. Zhang, Q. Bao, S. Wen, D. Tang, and D. Fan, "Mechanically exfoliated black phosphorus as a new saturable absorber for both Q-switching and mode-locking laser operation," Opt. Express **23**, 12823–12833 (2015).
18. Q. Sheng, M. Feng, W. Xin, H. Guo, T. Han, Y. Li, Y. Liu, F. Gao, F. Song, Z. Liu, and J. Tian, "Tunable graphene saturable absorber with cross absorption modulation for mode-locking in fiber laser," Appl. Phys. Lett. **105**, 041901 (2014).
19. S. Liu, Z. Li, Y. Ge, H. Wang, R. Yue, X. Jiang, J. Li, Q. Wen, and H. Zhang, "Graphene/phosphorene nano-heterojunction: facile synthesis, nonlinear optics, and ultrafast photonics applications with enhanced performance," Photon. Res. **5**, 662–668 (2017).
20. L. Titova, C. Pint, Q. Zhang, R. Hauge, J. Kono, and F. Hegmann, "Generation of terahertz radiation by optical excitation of aligned carbon nanotubes," Nano Lett. **15**, 3267–3272 (2015).
21. H. Yang, B. Fu, D. Li, Y. Tian, Y. Chen, M. Mattila, Z. Yong, R. Li, A. Hassanien, C. Yang, I. Tittonen, Z. Ren, J. Bai, Q. Li, E. I. Kauppinen, H. Lipsanena, and Z. Sun, "Broadband laser polarization control with aligned carbon nanotubes," Nanoscale **7**, 11199–11205 (2015).
22. L. Zhang, Y. Wu, L. Deng, Y. Zhou, C. Liu, and S. Fan, "Photodetection and photoswitch based on polarized optical response of macroscopically aligned carbon nanotubes," Nano Lett. **16**, 6378–6382 (2016).
23. Z. K. Tang, L. Zhang, N. Wang, X. X. Zhang, G. H. Wen, G. D. Li, J. N. Wang, C. T. Chan, and P. Sheng, "Superconductivity in 4 angstrom single-walled carbon nanotubes," Science **292**, 2462–2465 (2001).
24. N. Wang, Z. K. Tang, G. D. Li, and J. S. Chen, "Single-walled 4 Å carbon nanotube arrays," Nature **408**, 50–51 (2000).
25. Z. M. Li, Z. K. Tang, H. J. Liu, N. Wang, C. T. Chan, R. Saito, S. Okada, G. D. Li, J. S. Chen, N. Nagasawa, and S. Tsuda, "Polarized absorption spectra of single-walled 4 Å carbon nanotubes aligned in channels of an $AlPO_4$-5 single crystal," Phys. Rev. Lett. **87**, 127401 (2001).
26. A. Labropoulos, C. Veziri, M. Kapsi, G. Pilatos, V. Likodimos, M. Tsapatsis, N. K. Kanellopoulos, G. E. Romanos, and G. N. Karanikolos, "Carbon nanotube selective membranes with subnanometer, vertically aligned pores, and enhanced gas transport properties," Chem. Mater. **27**, 8198–8210 (2015).
27. Y. F. Mei, G. G. Siu, R. K. Y. Fu, P. K. Chu, Z. M. Li, J. P. Zhai, H. J. Liu, Z. K. Tang, C. W. Lai, and H. C. Ong, "Visible cathodoluminescence of 4 Å single-walled carbon nanotubes," Appl. Phys. Lett. **87**, 213114 (2005).
28. Q. Chen, Z. Wang, Y. Zheng, W. Shi, D. Wang, Y.-C. Luo, B. Zhang, J. Lu, H. Zhang, J. Pan, C.-Y. Mou, Z. Tang, and P. Sheng, "New developments in the growth of 4 angstrom carbon nanotubes in linear channels of zeolite template," Carbon **76**, 401–409 (2014).
29. F. X. Kartner, I. D. Jung, and U. Keller, "Soliton mode-locking with saturable absorbers," IEEE J. Sel. Top. Quantum Electron. **2**, 540–556 (1996).
30. D. Tang, B. Zhao, L. Zhao, and H. Tam, "Soliton interaction in a fiber ring laser," Phys. Rev. E **72**, 016616 (2005).

31. A. Grudinin and S. Gray, "Passive harmonic mode locking in soliton fiber lasers," J. Opt. Soc. Am. B **14**, 144–154 (1997).
32. N. Seong and D. Kim, "Experimental observation of stable bound solitons in a figure-eight fiber laser," Opt. Lett. **27**, 1321–1323 (2002).
33. S. Chouli and P. Grelu, "Rains of solitons in a fiber laser," Opt. Express **17**, 11776–11781 (2009).
34. S. Chouli and P. Grelu, "Soliton rains in a fiber laser: an experimental study," Phys. Rev. A **81**, 063829 (2010).
35. V. J. Matsas, T. P. Newson, D. J. Richardson, and D. N. Payne, "Selfstarting passively mode-locked fibre ring soliton laser exploiting nonlinear polarisation rotation," Electron. Lett. **28**, 1391–1393 (1992).
36. C. Gao, Z. Wang, H. Luo, and L. Zhan, "High energy all-fiber Tm-doped femtosecond soliton laser mode-locked by nonlinear polarization rotation," J. Lightwave Technol. **35**, 2988–2993 (2017).
37. P. Wang, C. Bao, B. Fu, X. Xiao, P. Grelu, and C. Yang, "Generation of wavelength-tunable soliton molecules in a 2-μm ultrafast all-fiber laser based on nonlinear polarization evolution," Opt. Lett. **41**, 2254–2257 (2016).
38. S. Liu, F. Yan, Y. Li, L. Zhang, Z. Bai, H. Zhou, and Y. Hou, "Noise-like pulse generation from a thulium-doped fiber laser using nonlinear polarization rotation with different net anomalous dispersion," Photon. Res. **4**, 318–821 (2016).